RESEARCH ARTICLE

Improved phase retrieval in holographic data storage based on a designed iterative embedded data

Changyu YU[1], Suping WANG[1], Ruixian CHEN[1], Jianying HAO[1], Qijing ZHENG[1], Jinyu WANG[1],

Xianying QIU[1], Kun WANG[1,2], Dakui LIN[1], Yi YANG[1], Hui LI[1,3], Xiao LIN (✉)[1,4], Xiaodi TAN (✉)[1]

1 Information Photonics Research Center, College of Photonic and Electronic Engineering, Fujian Normal University, Fuzhou 350117, China
2 Fujian Provincial Key Laboratory of Photonics Technology, Fuzhou 350117, China
3 Key Laboratory of OptoElectronic Science and Technology for Medicine of Ministry of Education, Fuzhou 350117, China
4 Wuhan National Laboratory for Optoelectronics, Wuhan 430074, China

Abstract Embedded data are used to retrieve phases quicker with high accuracy in phase-modulated holographic data storage (HDS). We propose a method to design an embedded data distribution using iterations to enhance the intensity of the high-frequency signal in the Fourier spectrum. The proposed method increases the anti-noise performance and signal-to-noise ratio (SNR) of the Fourier spectrum distribution, realizing a more efficient phase retrieval. Experiments indicate that the bit error rate (BER) of this method can be reduced by a factor of one after 10 iterations.

1 Introduction

With the development of information technology, extensive data are being generated at all times. Traditional data storage technology has difficulty coping with the increasing demand for data growth [1,2]. In 1963, Van Heerden formally proposed the concept of holographic data storage (HDS) [3]. HDS technology, as a three-dimensional volume storage technology, has garnered renewed attention because of its ultra-high storage density and ultra-fast data transfer rate [4–6].

Traditional HDS technology uses amplitude modulation, but the code rate is relatively low. In contrast, phase-modulated HDS can increase the code rate [7,8] and the

recording signal-to-noise ratio (SNR), which is conducive to further increasing the storage density; however, the camera cannot read the phase information directly. Typically, interferometric and non-interferometric phase-retrieval methods are used to decode the phase information. However, the interferometric phase decoding method suffers from problems, such as system complexity and instability of detection results [9–11], whereas non-interferometric phase-retrieval methods usually have a simpler and more stable detection system [12]. There exist many non-interferometric phase-retrieval methods, such as the ptycholographic iterative engine (PIE) algorithm [13,14], transport-of-intensity equation (TIE) [15,16], and iterative Fourier transform (IFT) algorithms [17,18]. This study employs the IFT algorithm to retrieve phase owing to its simpler and more stable system and single-shot operation.

The traditional IFT algorithm requires a multitude of iterations; thus, to reduce the number of iterations, the addition of available embedded data is proposed to enhance the constraint condition [19]. In actual experiments, iterations are typically more than simple simulations because the noise generated by the optical system and electrical components affect the Fourier intensity distribution [20]. The Fourier intensity distribution includes high and low-frequency information. Although the high-frequency information of the Fourier intensity aids in more accurate and faster phase retrieval, its intensity is weaker, and the noise immunity is worse than low-frequency information. Therefore, this paper proposes a method to encode embedded patterns to improve the SNR of high-frequency information in the Fourier intensity distribution and thus further increase the efficiency of phase retrieval.

2 Theory and methods

The model of the HDS and phase-retrieval system with embedded data is shown in Fig. 1.

In Fig. 1, the signal phase pattern is composed of unknown and embedded phase data. Unknown data refers to the valid information that needs to be recorded. Embedded data are known data, which can accelerate the phase reconstruction efficiency. In the recording process, the signal phase pattern was uploaded on the spatial light modulator (SLM) as the signal beam interferes with the reference beam, thereby recording a hologram in the media. Thereafter, in the reading process, the same reference beam illuminates the hologram, and the
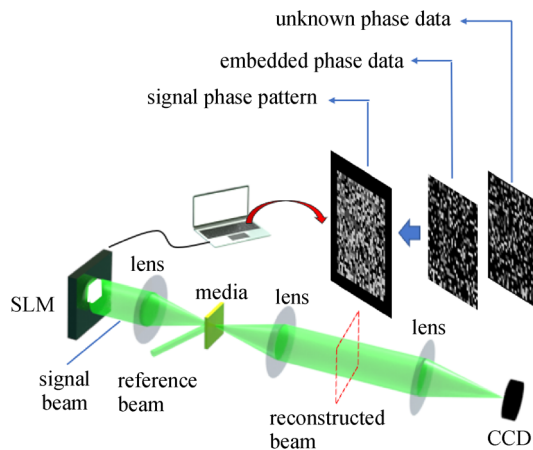
reconstructed beam is diffracted. Furthermore, to read out the phase information of the reconstructed beam, a single lens was used, and the charge-coupled device (CCD) captured the Fourier intensity distribution of the reconstructed beam. Finally, by using the IFT algorithm [12], the unknown phase data in the signal phase pattern was retrieved.

From previous studies, we discussed the proportion of embedded data, where 50% of the embedded data are appropriate [12]. Therefore, we used the 4-level phase data shown in Fig. 2(a) as the signal phase pattern, which is composed of 50% of unknown and embedded phase data each, as shown in Figs. 2(b) and 2(c), respectively. The Fourier intensity distribution captured by the CCD and its three-dimensional distribution is shown in Figs. 2(d) and 2(e), respectively. The red curve in Fig. 2(e) represents the intensity envelope in the Fourier plane.

In Fig. 2, it is intuitively evident that the high-frequency information intensity is relatively low compared to the low-frequency information intensity. The experiments performed indicated that the noise in Fourier intensity gradually decays from low to high-frequency, and thus a similar noise was added to the simulation, as shown in Fig. 3(a). The Fourier intensities before and after the addition of noise are shown in Figs. 3(b) and 3(c), and the corresponding three-dimensional envelope distributions are shown in Figs. 3(d) and 3(e). Furthermore, the calculated value of the SNR of the low-frequency part (in the red frame) is 7.52, and that of the high-frequency part (outside the red frame) is 0.38, which renders the high-frequency information susceptible when there is noise. High-frequency information can aid in retrieving the phase quicker with high accuracy; therefore, the aim of our
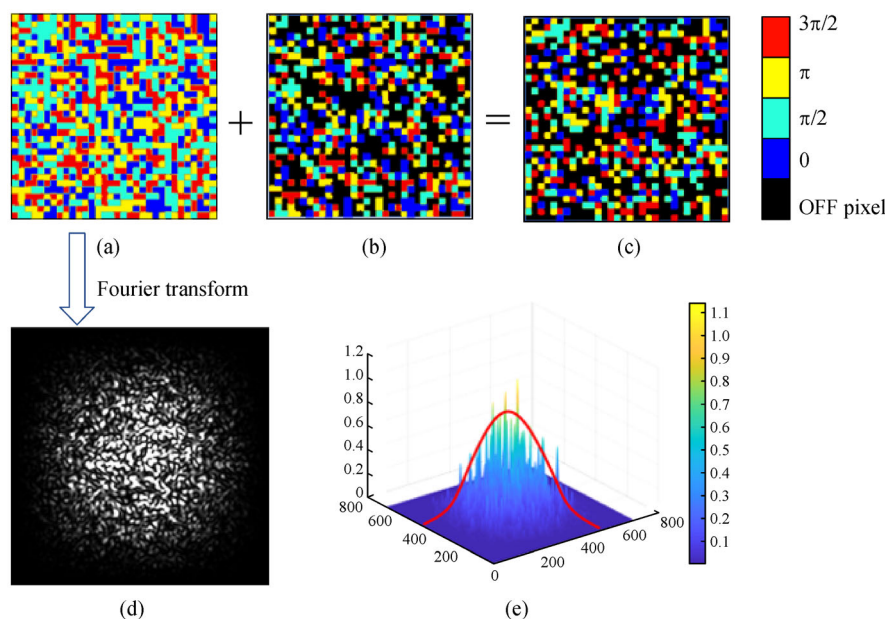

Fig. 1 Diagram of holographic data storage (HDS) and phase-retrieval system. SLM: spatial light modulator, CCD: charge-coupled device

Fig. 2 Process of generating intensity distribution in the Fourier plane. (a) Signal phase pattern. (b) Unknown phase data. (c) Embedded phase data. (d) Intensity in the Fourier plane. (e) Three-dimensional intensity distribution in the Fourier plane
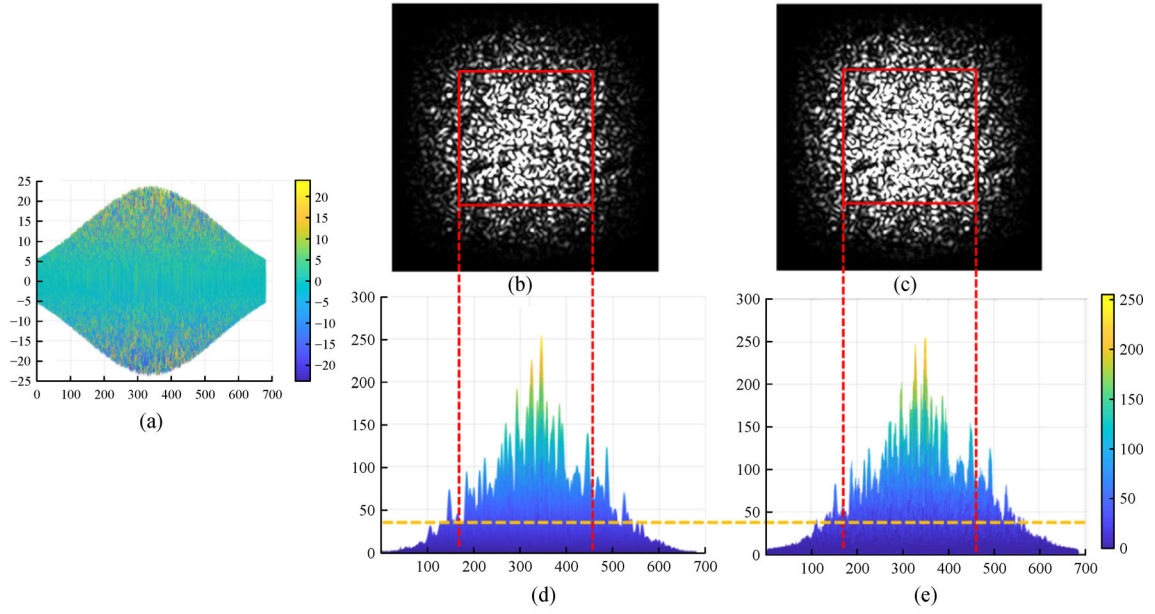
Fig. 3 Fourier intensity and its corresponding three-dimensional envelope distribution with or without noise. (a) Gaussian model noise. (b) and (d) Without noise. (c) and (e) With noise

method is to increase the intensity of the high-frequency information by encoding the embedded phase pattern.

The corresponding relationship between the phase pattern and the envelope intensity distribution is shown in Fig. 4.

Figures 4(a_1)–4(a_3) represent the unknown, previous embedded, and combined overall signal phase patterns, respectively. The envelope intensity distributions corresponding to the three-phase patterns are the red, blue, and solid yellow lines in Fig. 4(a), respectively. Figures 4(b_1) and 4(b_2) represent the new embedded and combined overall new signal phase patterns, respectively, and their corresponding envelope intensity distributions are represented by the blue and yellow dotted lines in Fig. 4(b), respectively.

In the actual experiment, we used a 4-level phase (0, $\pi/2$, π, $3\pi/2$) containing 50% embedded data. Moreover, oversampling should be used to avoid the phase gap effect
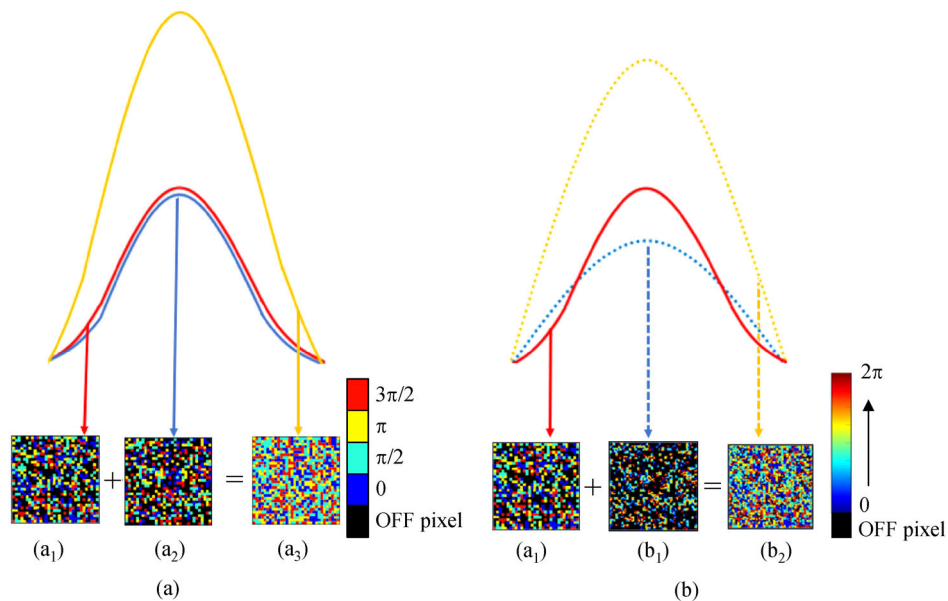

Fig. 4 Effect of changing the embedded phase pattern on the Fourier plane intensity distribution envelope. (a) Case before the change. (b) Case after the change

of adjacent pixels on the SLM. Typically, one phase of data should be displayed by 4×4 pixels on the SLM, such that the oversampling rate is 4. The spatial frequency on the SLM plane is the same for the unknown and previous embedded phase patterns. Therefore, their envelope intensity distributions are identical, as shown in Fig. 4(a), for the red and blue solid lines. We aim to design an envelope with a high-frequency, such as the blue dotted line shown in Fig. 4(b), and determine a new embedded phase pattern corresponding to it, as shown in Fig. 4(b$_1$). The space-frequency spectrum of embedded data we designed needs to be higher than that of the phase data page to improve the high-frequency component of the overall Fourier spectrum.

Because the Fourier intensity envelope is related to the phase pattern, after designing the intensity envelope about the embedded phase pattern, the embedded phase pattern itself can be obtained by using the IFT algorithm. Therefore, in our method, the embedded phase pattern is not assigned directly but is generated by iterative computing according to the designed intensity envelope of the embedded data.

The method to design a new embedded data phase pattern is as follows.

We used MATLAB software to generate a three-dimensional embedded data envelope intensity distribution with higher high-frequency as the constraint condition, as shown in Fig. 5(a).

Through the IFT algorithm, the previous embedded envelope intensity distribution, as shown in Fig. 5(b), was constrained and fitted to the designed three-dimensional envelope intensity distribution gradually, as shown in Fig. 5(a). Fitting is an iterative process; thus, typically, 20 iterations were required to complete the fitting, and in each iteration, a new embedded data envelope intensity distribution was obtained, as shown in Figs. 5(c) and 5(d), and new embedded data pattern corresponding to the envelope intensity distribution was recorded, to finally obtain 20 different embedded data patterns, as shown in Figs. 5(f) and 5(g). Our purpose was to determine the embedded phase pattern corresponding to the optimal envelope intensity distribution. By combining different new embedded data patterns with the same unknown data pattern, a series of different Fourier intensity distributions can be obtained, and thereafter, using the IFT algorithm [12], the phase retrieval results of different new embedded data patterns can be compared to determine the best new embedded data pattern.

Different new embedded data patterns affect the efficiency of phase retrieval. The specific algorithm for generating new embedded phase patterns is as follows:

In the first step, we consider an initial guess phase distribution of the embedded data φ_n, $n = 1, 2, 3,...$, which represents the number of iterations, and the position of the embedded data remains unchanged during the iteration. This results in a complex amplitude distribution U_n in the
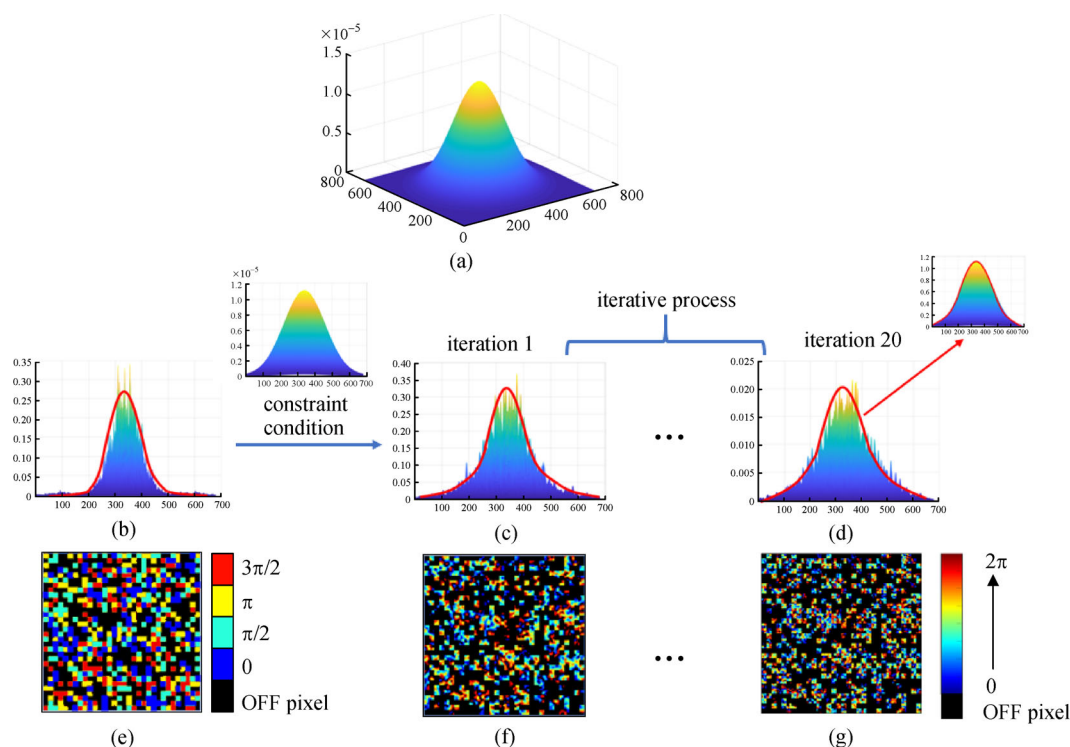

Fig. 5 Schematic diagram of generating new embedded data. (a) Constrained envelope distribution. (b) Previous embedded data envelope and its corresponding (e) embedded data pattern. (c) and (d) Envelope distribution under different iteration times and its corresponding (f) and (g) new embedded data patterns

object domain, as shown in Eq. (1).

$$U_n = \exp(i*\varphi_n).$$ (1)

This is followed by the second step, wherein we obtain a complex amplitude distribution V_n on the Fourier domain after the Fourier transform, as shown in Eq. (2).

$$V_n = \mathscr{F}\{U_n\} = |A_n| * \exp(i*\Phi_n),$$ (2)

where $\mathscr{F}\{\ \}$ represents the Fourier transform operator, and A_n and Φ_n represent the amplitude and phase, respectively.

Further, in the third step, we use the square root of the designed envelope intensity $\sqrt{I}$ to replace the amplitude A_n; thus, a new distribution V_n' can be obtained, as shown in Eq. (3).

$$V_n' = |\sqrt{I}| * \exp(i*\Phi_n).$$ (3)

Thereafter, in the fourth step, we continue to go through the inverse Fourier transform to obtain the new complex amplitude distribution U_n' on the object domain, as shown in Eq. (4).

$$U_n' = \mathscr{F}^{-1}\{V_n'\} = |A_n'| * \exp(i*\varphi_n'),$$ (4)

where $\mathscr{F}^{-1}\{\ \}$ represents the inverse Fourier transform operator, and A_n' and φ_n' represent the new amplitude and phase, respectively.

Finally, in the fifth step, phase-only is used as a constraint condition to rectify the complex amplitude distribution. Therefore, the amplitude was normalized to 1, resulting in a new distribution U_n'', as shown in Eq. (5).

$$U_n'' = \exp(i*\varphi_n''),$$ (5)

where φ_n'' is the new embedded phase pattern.

The afore described steps were repeated several times, and after each iteration, a new embedded data phase pattern was obtained; therefore, after several iterations, a series of different new embedded data phase patterns can be obtained.

3 Simulation and experimental results

We used a 32 × 32 signal phase pattern randomly with 4-level phase (0, $\pi/2$, π, $3\pi/2$), which contains 50% embedded data shown in Fig. 6(a), and each data was displayed in a 4 × 4 pixel block on the SLM with a pixel pitch of 20 μm. The pixel size of the CCD is 5.86 μm. According to the Nyquist sampling theorem, we chose two Nyquist size frequencies in the Fourier intensity shown in Fig. 6(b) for phase retrieval.

According to the flow shown in Fig. 5, we obtained new embedded data. To distinguish the previously embedded data from the new embedded data, they were named as the assigned embedded data and the iterative embedded data, respectively. The difference in the phase patterns between these two embedded data is shown in Fig. 7. Compared with the assigned embedded data, the iterative embedded data are more complex and finer because space complexity provides more high-frequency components.

Figure 8 shows the Fourier intensity distributions corresponding to the assigned embedded and iterative embedded data. It is evident that the details of the high-frequency information in Fig. 8(d) are more abundant than those in Fig. 8(b). Following this, we also evaluated the intensity of the high- and low-frequency signals in the Fourier plane from two perspectives. It was found that when the high-frequency intensity increased, the ratio of the high-frequency intensity to the total intensity increased; whereas, when the low-frequency intensity decreased, it resulted in a decrease in the ratio of the low-frequency intensity to the total intensity.

One Nyquist size-frequency is denoted as w, and we obtained two Nyquist size frequencies in the Fourier
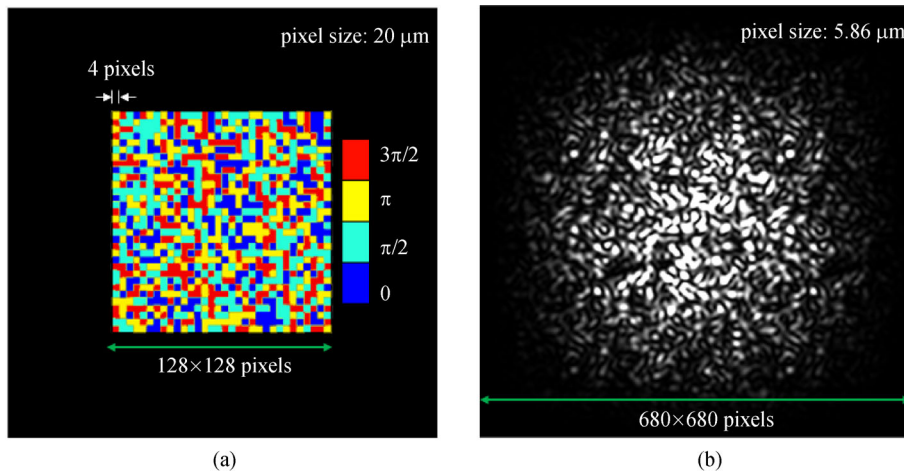

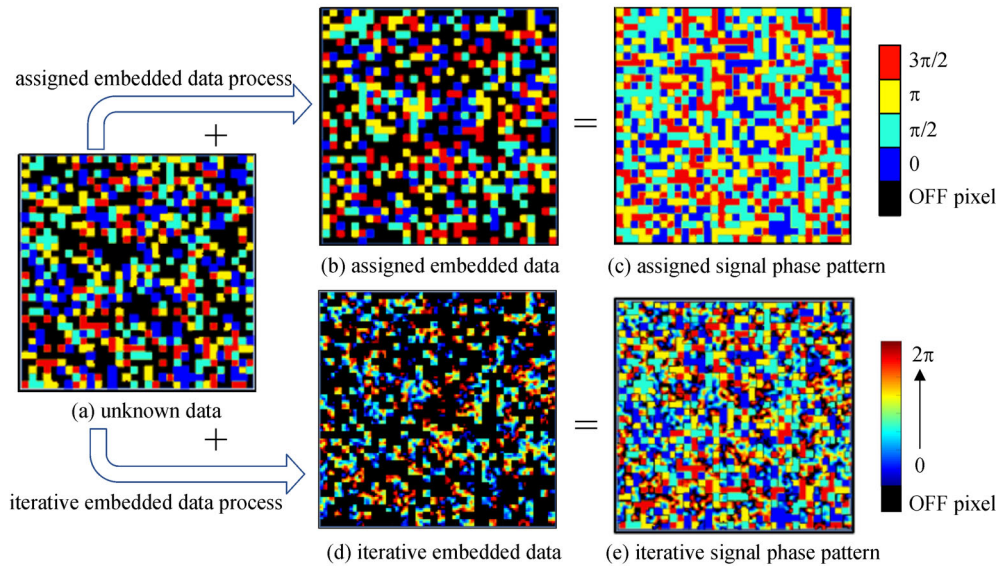**Fig. 6** (a) Signal phase pattern and (b) Fourier intensity with two Nyquist size frequencies

Fig. 7 Schematic diagram of phase pattern of object plane. (a) Unknown data. (b) Assigned embedded data. (c) Assigned signal phase pattern. (d) Iterative embedded data. (e) Iterative signal phase pattern
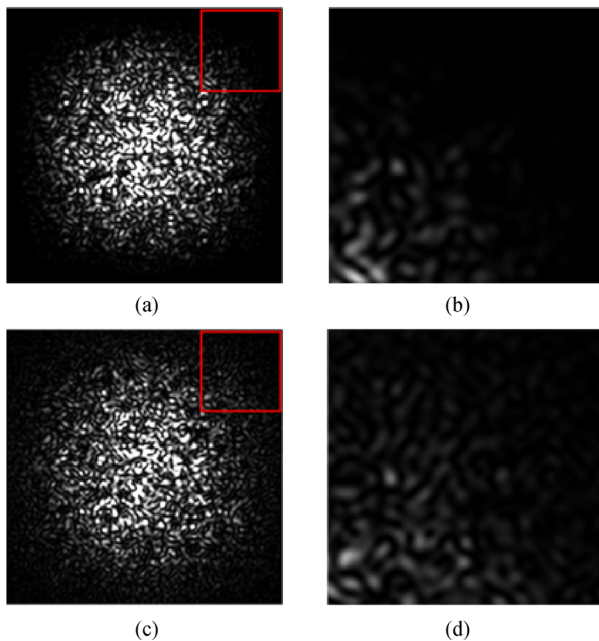

Fig. 8 Fourier intensity distributions corresponding to (a) assigned embedded data and (c) iterative embedded data, (b) and (d) are the enlargement of red boxes in (a) and (c), respectively

intensity, as shown in Fig. 9(a). Further, we calculated the average intensity of the two Nyquist size frequencies to be Q.

Furthermore, we calculated the intensity of the high-frequency information. The size of the yellow box gradually reduced from 1.9 to 1.5, and to express our choice of ideas more vividly; we only chose three yellow boxes of different sizes as the explanation. The yellow

boxes in Figs. 9(b)–9(d) show three different size windows: 1.9w, 1.7w, and 1.5w. Only the values outside these windows were retained, and thereafter the average intensity P was calculated.

In contrast, we calculated the intensity of the low-frequency information. The size of the red box was gradually increased from 0.1w to 0.5w, and similarly, three windows were selected as an illustration. The red boxes in Figs. 9(e)–9(g) are three different size windows of 0.1w, 0.3w, and 0.5w. Similarly, only the values inside these windows were retained, followed by the calculation of the average intensity R.

We calculated the proportional intensity coefficients E_1 and E_2 to evaluate the intensity distribution of the high- and low-frequency regions according to Eq. (6).

$$E_1 = \frac{P}{Q}, \quad E_2 = \frac{R}{Q}. \tag{6}$$

In the afore described embedded data algorithm, by controlling the number of iterations, we can obtain different embedded data envelope distributions corresponding to different iterative embedded data patterns, and thereby obtain a series of overall Fourier intensity distributions composed of different iterative embedded data patterns along with the same unknown data pattern. In Fig. 10, we selected three cases as illustrations.

In case 1, iterative embedded data are used to reduce the high-frequency Fourier intensity. Whereas in case 2, the high-frequency intensity was slightly greater than that in case 1 by using the assigned embedded data. Finally, in case 3, the iterative embedded data was changed to render the high-frequency of the Fourier intensity slightly greater
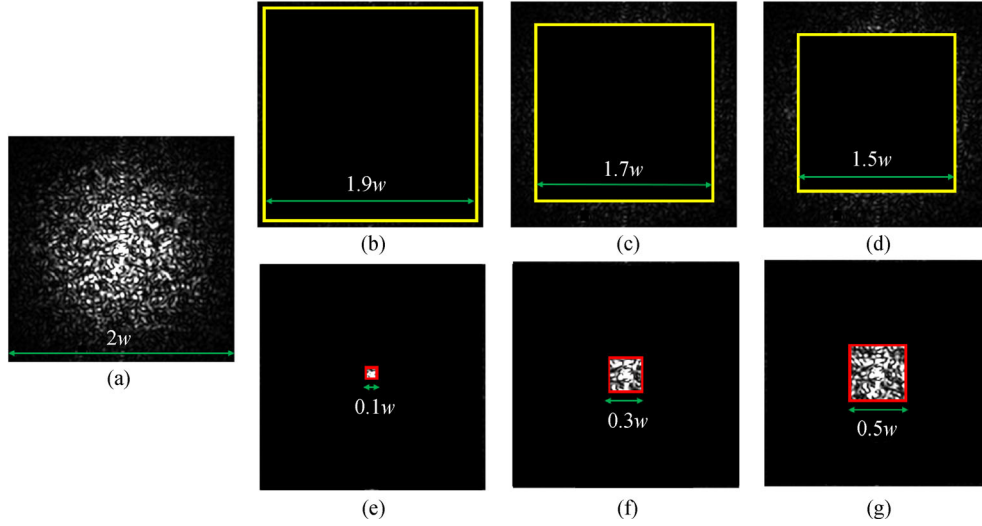
Fig. 9 Evaluate the intensity of the high-frequency and low-frequency. (a) $2w$. (b) $1.9w$. (c) $1.7w$. (d) $1.5w$. (e) $0.1w$. (f) $0.3w$. (g) $0.5w$
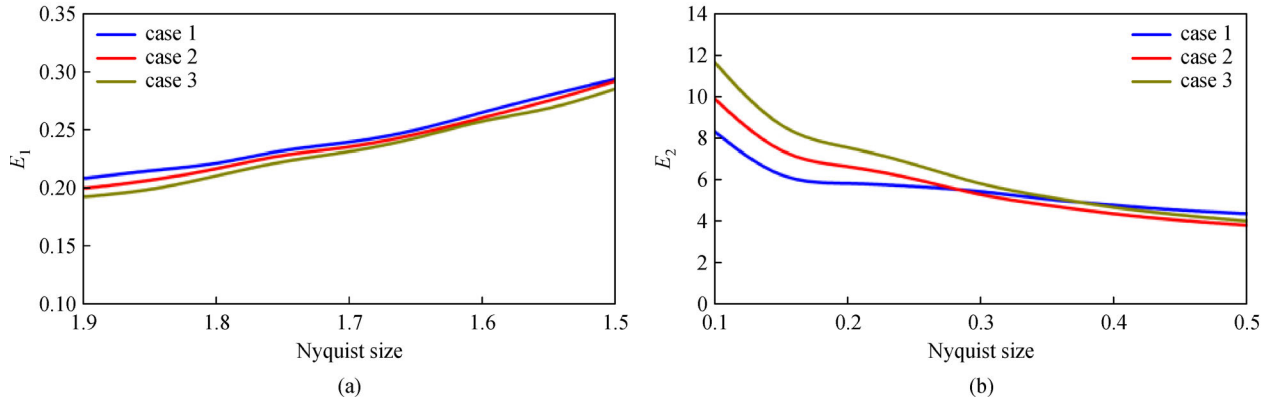

Fig. 10 Proportional intensity coefficients under different Nyquist spectrum. (a) E_1. (b) E_2

than that in case 2. Figures 10(a) and 10(b) show the proportional intensity coefficient curves corresponding to the calculation results of E_1 and E_2 in Eq. (6), respectively. A high value of E_1 along with a low value of E_2 indicates greater high-frequency information intensity, and vice-versa. E_1 and E_2 represent the same conclusions. However, the differences among the E_1 values were small, whereas the differences among the E_2 values were larger. The latter is more conducive to distinguishing different Fourier intensities; thus, we chose E_2 under 0.1 times the Nyquist size and used it to express the following calculation.

In the absence of noise, the assigned embedded and iterative embedded data are approximately the same for the phase retrieval because the SNR of high-frequency intensity does not decrease without noise, therefore strengthening of the high-frequency intensity is not required; thus, we only discuss the impact of the two forms of embedded data on phase retrieval in the presence of noise.

Noise exists in every process in the HDS system and deteriorates the phase retrieval directly. To simulate the influence of the experimental noise in the simulation, we added a certain amount of Gaussian model noise to the Fourier intensities formed by the assigned embedded data and iterative embedded data methods. The Gaussian model noise is shown in Fig. 3(a).

Thereafter, we used the IFT algorithm to calculate the bit error rate (BER) after 10 iterations with different Fourier intensities and determined the E_2 value corresponding to the minimum BER as shown in Fig. 11, and thus we determined the corresponding embedded data pattern at this time. Smaller the E_2 value, lower the low-frequency and higher the high-frequency. In Fig. 11, the black curve and red dot represent the phase-retrieval results corresponding to different iterative embedded and assigned embedded data patterns, respectively. When E_2 was 6.00, the BER of the iterative embedded data method was 0.033, while for E_2 of 8.31, and the BER was 0.064 in the case of the assigned embedded data method. It can be seen that phase retrieval is better when using the iterative embedded data method.

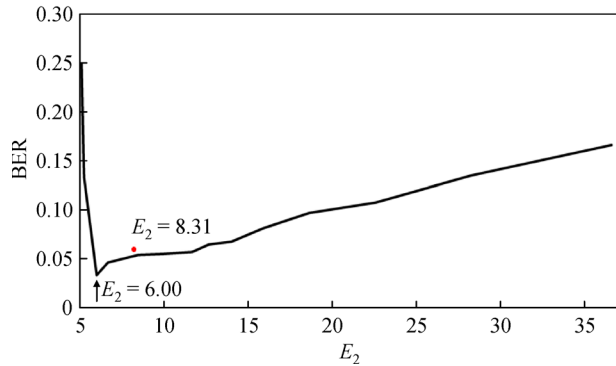In Fig. 12, we select two cases where the value of the

Fig. 11 Bit error rate (BER) curves under different Fourier intensities
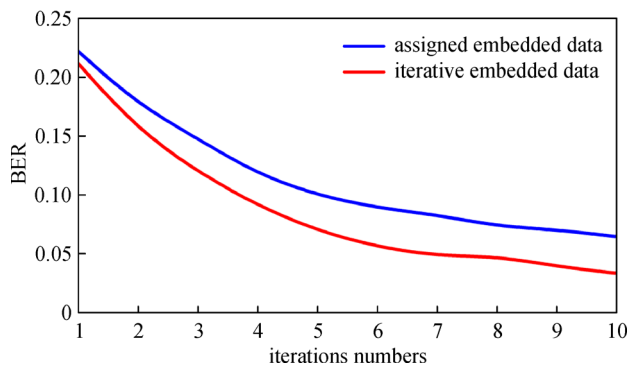

Fig. 12 Phase-retrieval results of simulation in different embedded data

assigned embedded data E_2 is 8.31, and the value of the iterative embedded data E_2 is 6.00, and compare the corresponding BER curves. When we use the iterative embedded data method, the phase retrieval is better because the E_2 value of the iterative embedded data method is lower than that of the assigned embedded method, which implies that the high-frequency intensity in the iterative embedded data method is higher. Under the same noise, the SNR of the assigned embedded data method was 6.0, while that of the iterative embedded data method was 6.6. Therefore, the convergence speed of the BER using the iterative embedded data method was faster.

The experimental setup of the non-interference phase-retrieval system is shown in Fig. 13.

We used the same parameters as those in the simulation. The wavelength of the laser was 532 nm, and its power was 300 mW. The SLM is a HAMAMATSU X10468-04 with a pixel pitch of 20 μm and a resolution of 792 × 600 pixels. The CCD is Thorlabs' DCC3260M, with pixel pitch of 5.86 μm, and resolution of 1936 × 1216 pixels. The media used was a PMMA photopolymer. The phase pattern was 32 × 32 phase data based on the combination of half embedded and half unknown phase data, and we used a block of 4 × 4 pixels to denote one-phase data. Finally, a 128 × 128 pixel phase pattern was loaded onto the SLM.

In the experiment, the Fourier intensity distributions corresponding to the assigned embedded data method and the iterative embedded data method are shown in Fig. 14.

It was experimentally verified that different intensity distributions were captured on the CCD. It is evident that the high-frequency detail information in Fig. 14(c) is more abundant. The phase-retrieval results corresponding to the assigned embedded data and the iterative embedded data are shown in Fig. 15.

In Fig. 15, after ten iterations, the iterative embedded data method can reduce the BER by approximately a factor of one. This proves that our proposed method of using embedded data to enhance the high-frequency intensity aids in improving phase retrieval.

4 Conclusions

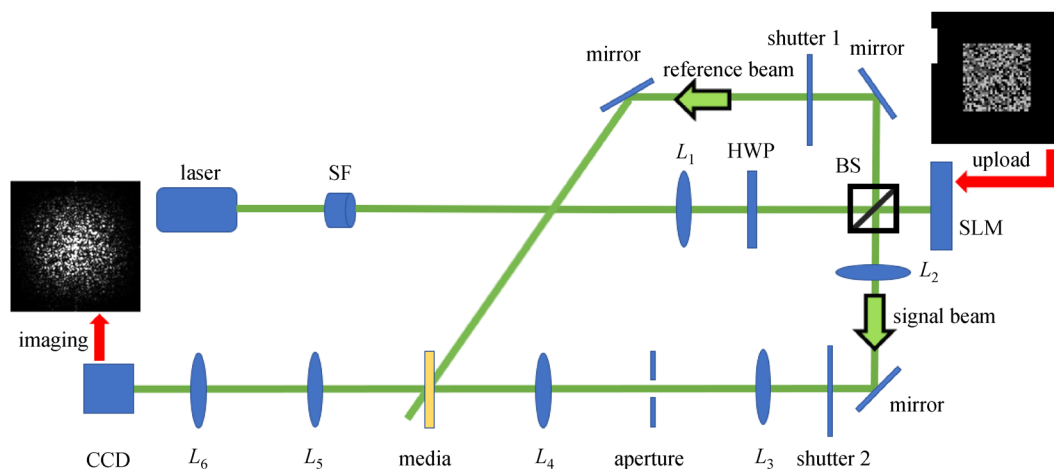In this study, we used the iterative embedded data method

Fig. 13 Experimental setup. SF: spatial filter, HWP: half-wave plate, BS: beam splitter, SLM: spatial light modulator, L_1–L_6: lens ($L_1 = 300$ mm, L_2–$L_5 = 150$ mm, $L_6 = 75$ mm)
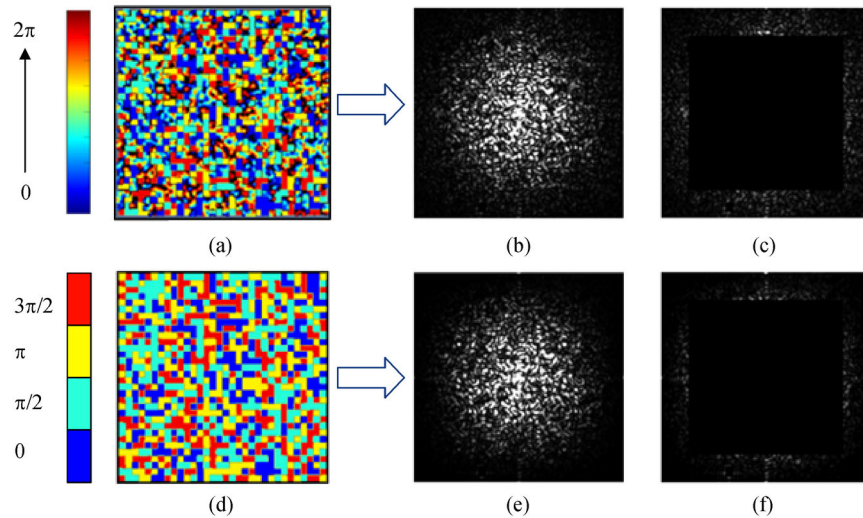
Fig. 14 Fourier intensity distribution in different embedded data. (a) Iterative embedded data. (d) Assigned embedded data. (c) and (f) are part of the high-frequency detail information in (b) and (e), respectively
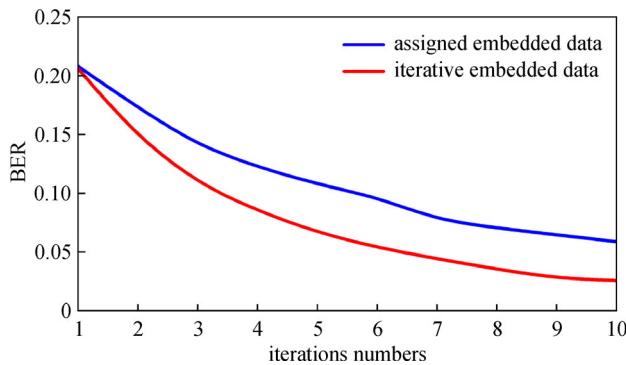

Fig. 15 Phase-retrieval results using different embedded data in the experiment

to increase the Fourier high-frequency intensity compared to the assigned embedded data method. When considering noise, the iterative embedded data method can reduce the BER by a factor of one, and the function of the known embedded data is further expanded, thus achieving faster retrieval of phase information.

Disclosures The authors declare no conflicts of interest.

References

1. Reinsel D, Gantz J, Rydning J. The Digitization of the World—From Edge to Core. IDC & Seagate: IDC White Paper, 2018

2. Haw M. Holographic data storage: the light fantastic. Nature, 2003, 422(6932): 556–558

3. Van Heerden P J. Theory of optical information storage in solids. Applied Optics, 1963, 2(4): 393–400

4. Horimai H, Tan X, Li J. Collinear holography. Applied Optics, 2005, 44(13): 2575–2579

5. Lin X, Hao J, Zheng M, Dai T, Li H, Ren Y. Optical holographic data storage—the time for new development. Opto-Electronic Engineering, 2019, 46(3): 180642

6. Lin X, Liu J, Hao J, Wang K, Zhang Y, Li H, Horimai H, Tan X. Collinear holographic data storage technologies. Opto-Electronic Advances, 2020, 3(3): 19000401

7. John R, Joseph J, Singh K. Holographic digital data storage using phase-modulated pixels. Optics and Lasers in Engineering, 2005, 43(2): 183–194

8. Psaltis D, Levene M, Pu A, Barbastathis G, Curtis K. Holographic storage using shift multiplexing. Optics Letters, 1995, 20(7): 782–784

9. He M, Cao L, Tan Q, He Q, Jin G. Novel phase detection method for a holographic data storage system using two interferograms. Journal of Optics. A, Pure and Applied Optics, 2009, 11(6): 065705

10. Jeon S H, Gil S K. 2-step phase-shifting digital holographic optical encryption and error analysis. Journal of the Optical Society of Korea, 2011, 15(3): 244–251

11. Xu X F, Cai L Z, Wang Y R, Meng X F, Zhang H, Dong G Y, Shen X X. Blind phase shift extraction and wavefront retrieval by two-frame phase-shifting interferometry with an unknown phase shift. Optics Communications, 2007, 273(1): 54–59

12. Lin X, Huang Y, Shimura T, Fujimura R, Tanaka Y, Endo M, Nishimoto H, Liu J, Li Y, Liu Y, Tan X. Fast non-interferometric iterative phase retrieval for holographic data storage. Optics Express, 2017, 25(25): 30905–30915

13. Pan X, Liu C, Lin Q, Zhu J. Ptycholographic iterative engine with self-positioned scanning illumination. Optics Express, 2013, 21(5): 6162–6168

14. Gureyev T E, Roberts A, Nugent K A. Phase retrieval with the transport-of-intensity equation: matrix solution with use of Zernike

polynomials. Journal of the Optical Society of America. A, Optics, Image Science, and Vision, 1995, 12(9): 1932–1942

15. Gureyev T E, Nugent K A. Rapid quantitative phase imaging using the transport of intensity equation. Optics Communications, 1997, 133(1–6): 339–346

16. Volkov V V, Zhu Y, De Graef M. A new symmetrized solution for phase retrieval using the transport of intensity equation. Micron (Oxford, England), 2002, 33(5): 411–416

17. Fienup J R. Phase retrieval algorithms: a comparison. Applied Optics, 1982, 21(15): 2758–2769

18. Fienup J R. Reconstruction of a complex-valued object from the modulus of its Fourier transform using a support constraint. Journal of the Optical Society of America. A, Optics and Image Science, 1987, 4(1): 118–123

19. Lin X, Huang Y, Li Y Y, Liu J, Liu J, Kang R, Tan X. Four-level phase pair encoding and decoding with single interferometric phase retrieval for holographic data storage. Chinese Optics Letters, 2018, 16(3): 032101

20. Liu J, Zhang L, Wu A, Tanaka Y, Shigaki M, Shimura T, Lin X, Tan X. High noise margin decoding of holographic data page based on compressed sensing. Optics Express, 2020, 28(5): 7139–7151
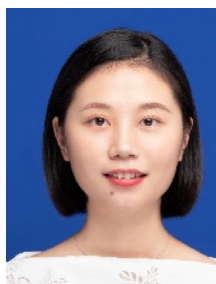
Changyu Yu received his B.E. degree in Department of Physical and Electronic Engineering from Gannan Normal University, China in 2018. He is currently working toward an M.S. degree in Optical Engineering at Information Photonics Research Center, Fujian Normal University, China. His current research interest is the optimization of non-interference phase retrieval algorithm.

Suping Wang received his B.E. degree in Optoelectronic Science from Fujian Normal University, China in 2019. He is currently working toward an M.S. degree in Optical Engineering at Information Photonics Research Center, Fujian Normal University, China. His current research interest is the analysis and compensation of optical field aberrations in holographic optical storage phase retrieval.

Ruixian Chen received her B.S. degree in College of Physics and Information Engineering from Quanzhou Normal University, China in 2019. She is currently working toward an M.S. degree in Optical Engineering at Information Photonics Research Center, Fujian Normal University, China. Her current research interest is focus dynamic sampling iterative phase retrieval for holographic data storage.

Jianying Hao is a Ph.D. student in Fujian Normal University, China. She received her M.S. degree in Optical Engineering from Beijing Institute of Technology, China in 2015. Her current research interests include holographic data storage, phase retrieval, computational optics and machine learning.

Qijing Zheng received her B.E. degree in Optoelectronic Information Science and Engineering from Jiangsu Normal University, China in 2019. She is currently working toward an M.S. degree in Optical Engineering at Information Photonics Research Center, Fujian Normal University, China. Her current research interests include holographic data storge and holographic phase retrieval.

Jinyu Wang received his B.E. degree in Optoelectronic Science from Fujian Normal University, China in 2018. He is currently working toward an M.S. degree in Optical Engineering at Information Photonics Research Center, Fujian Normal University, China. His current research interests include polarization holography, holographic storage and polarization sensitive media.

Xianying Qiu received her B.E. degree in Electronic Science and technology from Minjiang University, China in 2018. She is currently working toward an M.S. degree in Optical Engineering at Information Photonics Research Center, Fujian Normal University, China. Her current research interest is focus compensation of coaxial holographic storage system.

Kun Wang is an associate professor at Information Photonics Research Center, College of Photonic and Electronic Engineering, Fujian Normal University, China. She received her Ph.D. degree in 2015 from Department of Electronic Engineering, Tsinghua University, China. Her current research focuses on holographic data storage, freeform optical surface design, and polarization effects in InGaN-based solar cells.

Dakui Lin is an associate professor at College of Photonic and Electronic Engineering, Fujian Normal University, China. He obtained his Ph.D. degree from University of Science and Technology of China (USTC), China in 2020. His current research focuses on encrypted holographic data storage, diffraction grating and grating spectrometer.

Yi Yang received his B.S. degree in physics from Central China Normal University, China in 2015, and Ph.D. degree from School of Optical and Electronic Information, Huazhong University of Science and Technology, China in 2020. His current research interests include holographic optical data storage system and digital signal processing.

Hui Li is a full professor in Optics and Optical Engineering at Fujian Normal University, China. He received his Ph.D. degree in Optical Engineering from Zhejiang University, M.S. degree in Optics from Fujian Normal University and B.S. degree in Physics from Peking University, China. His areas of research interest include optics and optical engineering, information processing, optoelectronic sensing, photoacoustic imaging for medical applications. He got 4 projects supported by the National Natural Science Foundation of China. He had 130 papers published and 5 patents authorized.

Xiao Lin received his Ph.D. degree from Beijing Institute of Technology, China in 2018. Now he is an associate professor at Fujian Normal University, China. His research fields are holographic data storage, computing phase imaging, machine learning, 3D display. He published over 80 articles in journals and conferences and gave 6 invited talks. He is the member of OSA, SPIE, COS, and CSOE, and the peer reviewer in *Optics Letters*, *Applied Optics*, etc.

Xiaodi Tan graduated from Optical Department of Shandong University, China in 1984, he obtained his Master's Degree from Optical Engineering Department of Beijing Institute of Technology, China. His doctoral thesis on "Optical Secure Holographic Storage Systems" was completed at The University of Tokyo, Institute of Industrial Science, in the Laboratory of Kuroda-Shimura, Japan in 2001. He was a Senior Engineer of the Technology Division in OPTWARE Corporation, researching and developing the next generation of optical storage systems. And he was a Senior Technology Analyst, Distinguished Engineer and Optical Technology Manager of Core Device Development Group in Sony Corporation. He was a professor at School of Optoelectronics of Beijing Institute of Technology from 2012 to 2017. And now he is a professor at College of Photonic and Electric Engineering of Fujian Normal University, China. His research interests are in information optics: holographic data storage, optical information display, optical devices, etc.